© 2020. Published by The Company of Biologists Ltd | Journal of Cell Science (2020) 133, jcs237800. doi:10.1242/jcs.237800

SHORT REPORT

SPECIAL ISSUE: CELL BIOLOGY OF THE IMMUNE SYSTEM

Macrophages show higher levels of engulfment after disruption of *cis* interactions between CD47 and the checkpoint receptor SIRPα

Brandon H. Hayes[1,2,*], Richard K. Tsai[1,2,*], Lawrence J. Dooling[1], Siddhant Kadu[1], Justine Y. Lee[1], Diego Pantano[1], Pia L. Rodriguez[1], Shyamsundar Subramanian[1], Jae-Won Shin[1,3] and Dennis E. Discher[1,2,3]

ABSTRACT

The macrophage checkpoint receptor SIRPα signals against phagocytosis by binding CD47 expressed on all cells – including macrophages. Here, we found that inhibiting *cis* interactions between SIRPα and CD47 on the same macrophage increased engulfment ('eating') by approximately the same level as inhibiting *trans* interactions. Antibody blockade of CD47, as pursued in clinical trials against cancer, was applied separately to human-derived macrophages and to red blood cell (RBC) targets for phagocytosis, and both scenarios produced surprisingly similar increases in RBC engulfment. Blockade of both macrophages and targets resulted in hyper-phagocytosis, and knockdown of macrophage-CD47 likewise increased engulfment of 'foreign' cells and particles, decreased the baseline inhibitory signaling of SIRPα, and linearly increased binding of soluble CD47 in *trans*, consistent with *cis-trans* competition. Many cell types express both SIRPα and CD47, including mouse melanoma B16 cells, and CRISPR-mediated deletions modulate B16 phagocytosis, consistent with *cis-trans* competition. Additionally, soluble SIRPα binding to human CD47 displayed on Chinese hamster ovary (CHO) cells was suppressed by SIRPα co-display, and atomistic computations confirm SIRPα bends and binds CD47 in *cis*. Safety and efficacy profiles for CD47–SIRPα blockade might therefore reflect a disruption of both *cis* and *trans* interactions.

KEY WORDS: Phagocytosis, Inhibitory receptor, Erythrocyte, 'Marker of self'

INTRODUCTION

Immune cells come in frequent contact with cells that either originate from the same organism, and are thus 'self', or else are 'foreign', such as microbes. 'Self' recognition occurs in part through interactions that ultimately inhibit immune activation. An important clinical example in anti-cancer therapy is the inhibitory T-cell receptor PD-1 (also known as PDCD1) that interacts with PD-L1 (also known as CD274) on 'self' cells in parallel with T-cell receptor interactions; if the latter activates a T-cell to attack, then PD-1 engagement effectively pacifies the T-cell. Blocking this 'checkpoint' by systemic injection of inhibitory antibodies (e.g. anti-PD-1 antibody) leads to elimination of tumors in a fraction of otherwise untreatable patients, with the best responses occurring against tumors that are highly mutated (i.e. 'foreign') (Mandal et al., 2019). Activation-dominated-by-inhibition applies also to macrophages; these phagocytes express the inhibitory receptor SIRPα (signal regulatory protein-α, CD172A) that engages in *trans* with the 'marker of self' CD47, which is expressed on all cells (Oldenborg et al., 2000). CD47 is also present on the macrophage, which raises the possibility of *cis* binding of SIRPα to CD47 within the same membrane, as has been postulated for other receptors on other immune cells (Doucey et al., 2004).

When a macrophage engages a 'self' cell, a phagocytic synapse forms in which *trans* binding of SIRPα to CD47 leads to local accumulation of SIRPα and phosphatase-mediated signaling that opposes engulfment ('eating') of 'self' cells including tumor cells (Fig. 1Ai, upper) (Oldenborg et al., 2000; Tsai and Discher, 2008; Weiskopf et al., 2013; Chowdhury et al., 2019). Phagocytosis-activating interactions occur in parallel, with the clearest pathway involving Fc-receptors (FcRs) that bind and organize IgG-type antibodies on a target cell (Lopes et al., 2017; Bakalar et al., 2018). IgG-opsonized targets activate the actomyosin tension that makes phagocytic internalization a highly efficient process – especially when CD47 is absent from a phagocytic target or else blocked with anti-CD47, including Fc-deficient $F(ab')_2$ (Tsai and Discher, 2008; Sosale et al., 2015). However, any effect of anti-CD47 binding to macrophage CD47 remains unclear.

One humanized anti-CD47 IgG has been infused recently at high doses into lymphoma patients in combination with a second IgG (i.e. anti-CD20, Rituximab) that opsonizes the cancer cells to activate macrophages. 32% of all patients were found to exhibit a complete response (Fig. 1Ai, lower) (Advani et al., 2018), similar to that achieved when blocking PD-1 on other tumor types (Borghaei et al., 2015). Safety concerns with intravenous anti-CD47 include loss of blood cells, especially loss of red blood cells (RBCs), which is seen across various clinical trials (Sikic et al., 2018; summarized in Andrechak et al., 2019) (Fig. 1Aii). Anti-CD47 binds CD47 on all cells, and injection of anti-mouse CD47 antibody in common mouse strains also causes anemia (Ingram et al., 2017), as does CD47 knockout in at least one strain of mouse (Oldenborg et al., 2002). Splenic macrophages engulf CD47-deficient RBCs when injected in normal mice (Oldenborg et al., 2000), consistent with anti-CD47 blockade (Ingram et al., 2017), but no clinical or mouse study has determined the factors that activate blood cell engulfment. We hypothesized that CD47 is highly abundant on macrophages and that it modulates phagocytosis through a *cis* interaction with SIRPα. The following results show that either blocking or depleting CD47 on macrophages causes these cells to engulf more targets in phagocytosis assays, and depletion also suppresses a basal level of inhibitory signaling by SIRPα. Studies of binding and of a SIRPα-expressing cancer line additionally prove consistent with molecularly detailed simulations of a *cis* interaction between CD47 and SIRPα on the same cell surface.

[1]Molecular & Cell Biophysics Lab, University of Pennsylvania, Philadelphia, PA 19104, USA. [2]Graduate Group in Bioengineering, University of Pennsylvania, Philadelphia, PA 19104, USA. [3]Graduate Group in Pharmacology, University of Pennsylvania, Philadelphia, PA 19104, USA.

*These authors contributed equally to this work

B.H.H., 0000-0002-9099-201X; R.K.T., 0000-0002-3464-3210; L.J.D., 0000-0002-1688-2066; S.S., 0000-0002-2882-738X; D.E.D., 0000-0001-6163-2229

Received 14 August 2019; Accepted 20 December 2019

Journal of Cell Science (2020) 133, jcs237800. doi:10.1242/jcs.237800

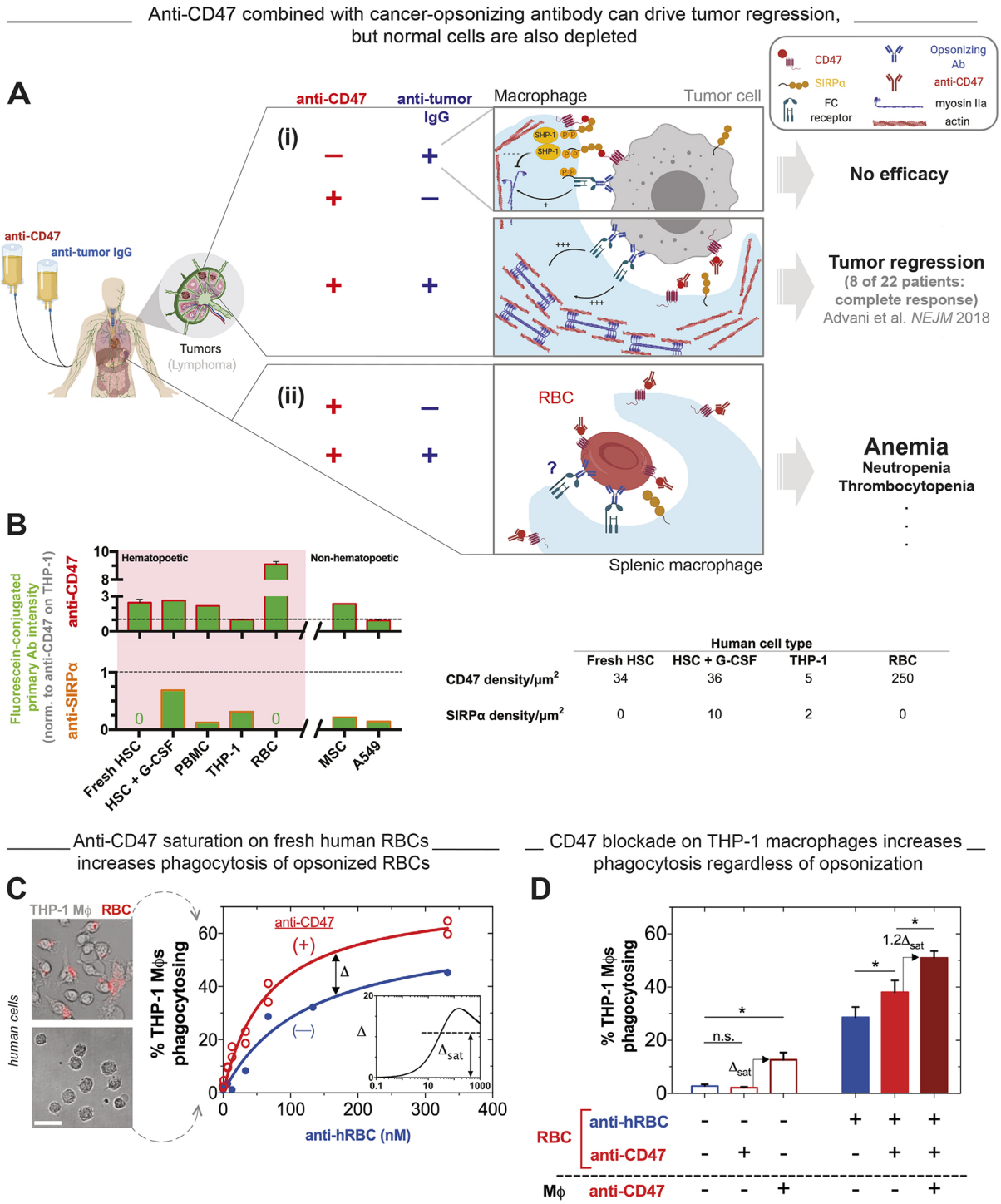

Fig. 1. Treatment of macrophages with anti-CD47 increases phagocytosis. (A) (i) Recent trials of anti-CD47 therapies have shown efficacy only when combined with anti-cancer opsonizing antibodies. In particular, a primary mechanism of anti-CD20-mediated clearance of B-cell lymphoma is via IgG-activated phagocytosis by liver macrophages (i.e. Kupffer cells), requiring B-cells to enter the blood circulation (Montalvao et al., 2013). (ii) Blockade of CD47 often causes loss of blood cells, especially RBCs, presumably through splenic macrophages. (B) Bar graph, CD47 and SIRPα expression on diverse human-derived cell types, including hematopoietic cells (stem cells, HSCs; PBMC, peripheral blood monocytic cells, a THP-1 monocyte line and RBCs), plus mesenchymal stem cells (MSCs), and A549 lung adenocarcinoma cells. HSCs were differentiated to myeloid cells by treatment with G-CSF according to Shin et al. (2013). Quantification by flow cytometry used primary antibodies (B6H12, SEC72 clones) labeled with fluorescein (mean±s.e.m. for all results; n=4). Table, molecular density estimates for CD47 and SIRPα on several hematopoietic cell types based on Subramanian et al. (2007). (C) Phagocytosis assays used THP-1 macrophages (Mϕ) and human RBC (hRBC) opsonizing antibody with or without anti-CD47 (B6H12) at saturating level. Engulfment of fluorescent hRBCs was confirmed with a secondary antibody against anti-hRBC. Microscopy fields are randomly selected, and >200 macrophages counted (n=3, mean±s.d.). Hyperbolic fits $y=A\,x/(K+x)$ of each data set [(A,K): (74%, 67 nM) for anti-CD47, (63%, 125 nM) for control; R^2>0.97] give the (inset) difference curve with the difference between A values as Δ_{sat}. Scale bar: 20 µm. (D) Anti-CD47 pre-incubated for 45 min with THP-1 macrophages (and excess removed) increased phagocytosis of target hRBCs, independently of hRBC opsonization. Results are mean±s.d., n=3. *P<0.03, n.s., not significant.

Journal of Cell Science (2020) 133, jcs237800. doi:10.1242/jcs.237800

RESULTS AND DISCUSSION

Blocking CD47 on macrophages increases phagocytosis

To first determine relative levels of CD47 and SIRPα on diverse cell types, primary antibodies labeled with fluorescein were used in flow cytometry quantification (Fig. 1B; Fig. S1A). Relative to CD47 levels on human monocytic THP-1 cells, CD47 levels were within 2–3-fold for most other hematopoietic and non-hematopoietic cell types. RBCs are an exception, but ∼10-fold higher levels are consistent with an 80–90% excess of CD47 relative to levels needed to inhibit engulfment by macrophages (Tsai and Discher, 2008). SIRPα expression was expectedly restricted among hematopoietic cells to phagocytes, including human THP-1 macrophages, cytokine (granulocyte colony stimulating factor; G-CSF)-differentiated human stem cells (HSCs+G-CSF), and peripheral blood mononuclear cells (PBMCs) (Fig. 1B); the SIRPα levels found on human mesenchymal stem cells (MSCs) and A549 lung cancer cells agrees with those found in past studies (Vogel et al., 2003; Sosale et al., 2016). Transcriptome analyses further showed that SIRPα was expressed in some mouse cancer cell types as well as primary mouse macrophages, which have an expression profile similar to THP-1 macrophages (Fig. S1B). Nonetheless, the protein analyses showed that CD47 exceeds SIRPα by 3:1 or greater for all cell types, and so all of these cell types should robustly signal 'self' to macrophages.

To study anti-CD47 blockade effects on phagocytosis of human RBCs (hRBCs) by human macrophages, fresh hRBCs were pre-incubated with opsonizing anti-hRBC at various levels, with or without saturating levels of anti-CD47, and then added to THP-1 macrophages (Fig. 1C; Fig. S2A–D). Engulfment of opsonized hRBCs increases with anti-CD47 treatment, and saturation binding curves reveal a ∼2-fold higher half-max activity and >10% higher saturation (Δ_{sat}) (Fig. 1C). However, for hRBCs without any opsonization (i.e. anti-hRBC=0), anti-CD47 does not promote phagocytosis (Fig. 1C; Fig. S2D). This is surprising because if freshly isolated RBCs display an endogenous opsonizing signal of relevance to the effects of systemic blockade, then anti-CD47 should increase *in vitro* engulfment. The anemia and loss of other blood cells in clinical blockade of CD47 (Fig. 1Aii) thus motivate a search for other mechanism(s).

Anti-CD47 infused intravenously should bind CD47 on macrophages in the spleen, among other accessible tissues. THP-1 macrophages were therefore pre-incubated with anti-CD47, and excess antibody was removed before assaying phagocytosis. Engulfment of hRBCs increased even with non-opsonized hRBCs (Fig. 1D, left; Fig. S2A,B), and addition of anti-hRBC to hRBCs also increased engulfment, with maximal levels seen for anti-CD47 pre-bound to both THP-1s and hRBCs (Fig. 1D, right; Fig. S2A). The increased percentage of macrophages engulfing hRBCs was also accompanied by more hRBCs being engulfed per macrophage (Fig. S2A, top); THP-1s only phagocytosed ∼1 hRBC in the absence of any added antibodies, whereas ∼2 hRBCs were often engulfed per macrophage under conditions of maximal engulfment. Regardless, pre-binding of anti-CD47 to THP-1 macrophages tended to increase the percentage of engulfment (i.e. percentage of cells with internalized particles) by an amount similar to that achieved with anti-CD47 blockade on fully opsonized hRBCs (Fig. 1D, Fig. S2C). The typical increase (∼Δ_{sat} in Fig. 1C,D) underscores the relatively large effect of blocking CD47 on the macrophage. Therefore, hyper-phagocytosis of opsonized targets is a result of blockade of both the target and the macrophage, based potentially on inhibition of the *cis* CD47-SIRPα interaction.

Knockdown of macrophage CD47 increases engulfment and decreases basal signaling

Anti-CD47 on a macrophage could conceivably dissociate and bind an RBC target and vice versa – although symmetric saturation of both cells will eliminate exchange and was seen to maximize engulfment (Fig. 1D). To achieve a more-stable asymmetric blockade effect, CD47 was suppressed in THP-1 macrophages using shRNA, without affecting SIRPα (Fig. S3A,B). Phagocytosis was assayed (again per macrophage as in Fig. S2A, top) with IgG-opsonized sheep red blood cells (ShRBCs) as targets for knockdown (KD) and wild-type (WT) THP-1 macrophages; it is already known that sheep CD47 does not bind human SIRPα (Tsai and Discher, 2008). ShRBCs were engulfed ∼30% more per KD macrophage compared to WT and to KD controls (Fig. 2A; Fig. S3C). Compared to the ShRBCs, opsonized human-RBCs show a decrease in 'self'-inhibited background engulfment by both WT and KD THP-1 macrophages, following the expected trends (Fig. S3D). IgG-opsonized microbeads were likewise engulfed at higher levels per KD macrophage (Fig. 2A). Macrophages are thus hyper-phagocytic if their CD47 is either blocked with an antibody (Fig. 1D) or knocked down, especially when CD47 on the target is lacking.

Phosphorylation of tyrosine residues in the cytoplasmic immunoreceptor tyrosine-based inhibiting motif (ITIM) of SIRPα increases when CD47 on a phagocytic target binds SIRPα in *trans*, with phospho-SIRPα activating a downstream phosphatase (Veillette et al., 1998) that turns off actomyosin (Fig. 2A, images) and thereby turns off efficient engulfment (Tsai and Discher, 2008). Basal phosphorylation of SIRPα in the absence of phagocytic targets remains unexplained (Oldenborg et al., 2000; Ide et al., 2007; Tsai and Discher, 2008), but we observe lower levels of phospho-SIRPα in CD47 KD THP-1-macrophages than in WT, with a linear increase from zero as a function of CD47 levels (Fig. 2B). Note that the deepest KD essentially inverts the CD47:SIRPα stoichiometry from ∼3:1 excess CD47 to >2:1 excess SIRPα (Fig. 1B; Fig. S3B). Decreased basal signaling with CD47 depletion and the increased phagocytosis led us to hypothesize that CD47 on a WT macrophage binds in *cis* on the same macrophage membrane to SIRPα.

Competitive binding between CD47 and SIRPα in *cis* versus *trans*

To quantify *cis* binding in competition with *trans* binding, binding curves were generated for soluble fluorescent CD47 added to WT and KD THP-1 macrophages. Flow cytometry reveals a saturable, moderate affinity (1.6 µM) interaction for SIRPα on WT cells (Fig. 2Ci). However, a substantial knockdown of CD47 (to ∼13%) strongly increases this apparent binding affinity to 0.26 µM (Fig. 2Ci), and intermediate knockdown shows that the apparent dissociation constants (K_d) increase linearly with CD47 levels on the macrophage (Fig. 2Cii). Our previous measures of soluble SIRPα binding to CD47 on hRBCs, which lack any *cis* interactions (Fig. 1Ai), gave K_d=0.2 µM (Sosale et al., 2015); such a value matches the intercept of the THP-1 results. The same studies of hRBCs also showed anti-CD47 (B6H12 clone) binds as expected, with much higher affinity (40 nM).

Mathematically, *trans* or *cis* concentrations of CD47 (C_t, C_c, respectively) compete for a single site on macrophage SIRPα (Fig. 2Cii, inset). Given association constants K_c and K_t, the fractional occupation of SIRPα by *trans*-CD47 is:

$$\theta = \frac{K_t C_t}{1 + K_c C_c + K_t C_t} \quad (1)$$

Journal of Cell Science (2020) 133, jcs237800. doi:10.1242/jcs.237800

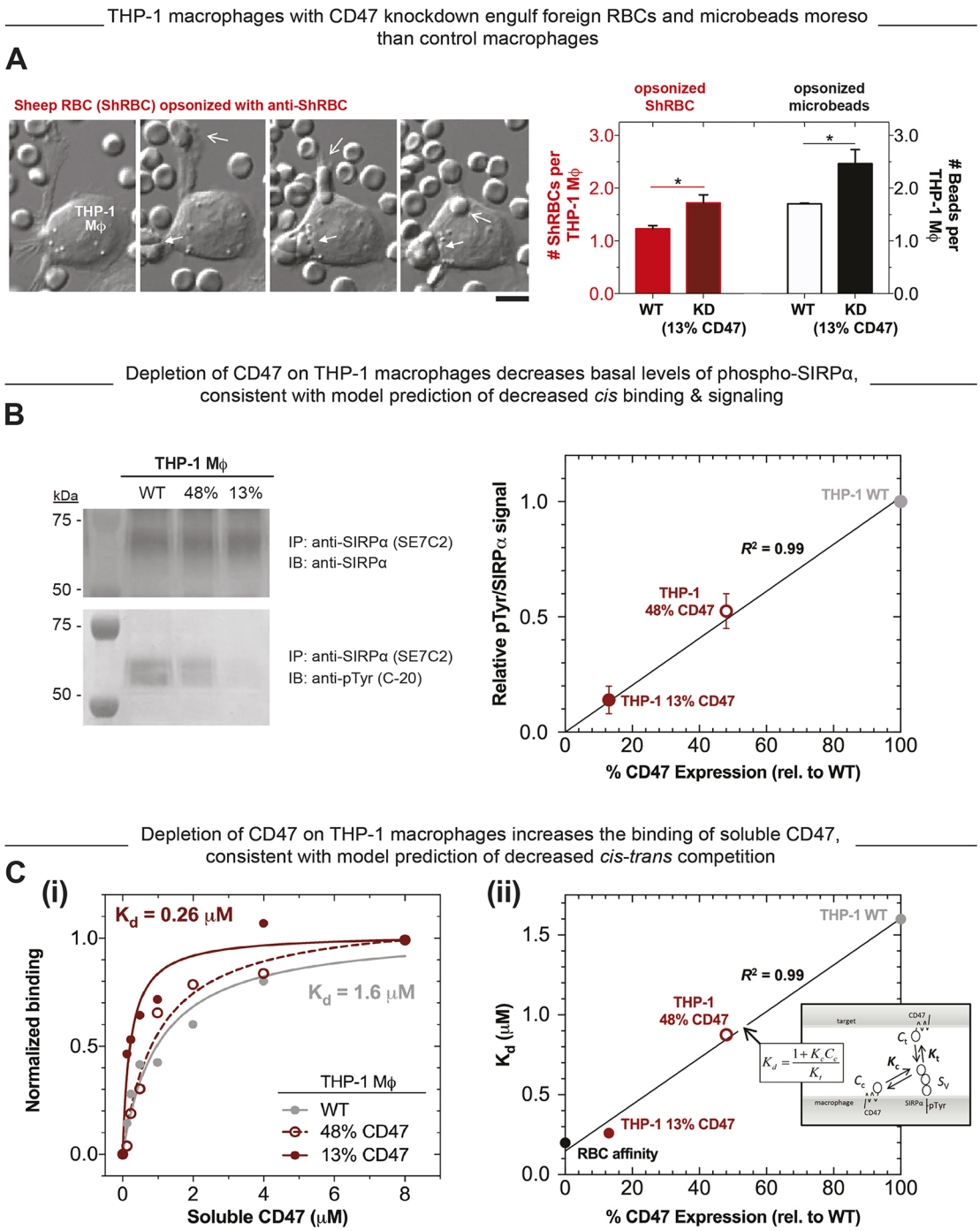

Fig. 2. Depleting CD47 on macrophages increases engulfment activity, decreases SIRPα signaling and increases SIRPα affinity. (A) Stable knockdown of CD47 on THP-1 macrophages to 48% or 13% of wild-type (WT) levels was used to phenocopy anti-CD47 effects. Phagocytosis assays with WT or knockdown (KD) THP-1 cells used IgG-opsonized sheep RBCs (ShRBCs) or IgG-opsonized streptavidin microbeads. Microscopy fields randomly selected and 200 macrophages counted (n=3, mean±s.e.m.). Images, engulfment of ShRBCs. Arrows denote phagocytic events. Scale bar: 10 µm. THP-1 cells with 13% CD47 levels had higher levels of engulfment than WT (~40%). *P<0.03. (B) SIRPα immunoprecipitation from lysates of THP-1 macrophages under basal conditions using anti-SIRPα (SE7C2 clone) and immunoblotted for phospho-tyrosine (pTyr; C-20 clone) (n=3, mean±s.e.m.). The normalized SIRPα pTyr signal increases linearly from zero in relation to the CD47 level. (C) (i) To quantify the effective affinity of CD47 for SIRPα in *trans* on WT and KD THP-1 macrophages, binding of fluorescent soluble CD47 was measured by flow cytometry and normalized to 8 µM data. All data fits $y=A\,x/(K_d+x)$ (R^2>0.93) for apparent dissociation constants (K_d). (ii) K_d increases linearly in relation to the CD47 level, and the non-zero intercept corresponds to the highest affinity for CD47–SIRPα as measured for human RBCs that lack SIRPα (Fig. 1B).

We write θ as a hyperbolic function of C_t (per Fig. 2Ci) by defining:

$$K_d = \frac{1 + K_c C_c}{K_t} \quad (2)$$

Linearity in C_c fits the CD47-dependence of K_d (Fig. 2Cii) and linear signaling (Fig. 2B). Furthermore, K_d=(k_{off}/k_{on}) and agrees with the finding that soluble CD47 binds slower in *trans* to WT THP-1 cells, with k_{on} of 0.65 min^{-1}, compared to 0.36 min^{-1} for KD cells (Fig. S3E).

Journal of Cell Science (2020) 133, jcs237800. doi:10.1242/jcs.237800

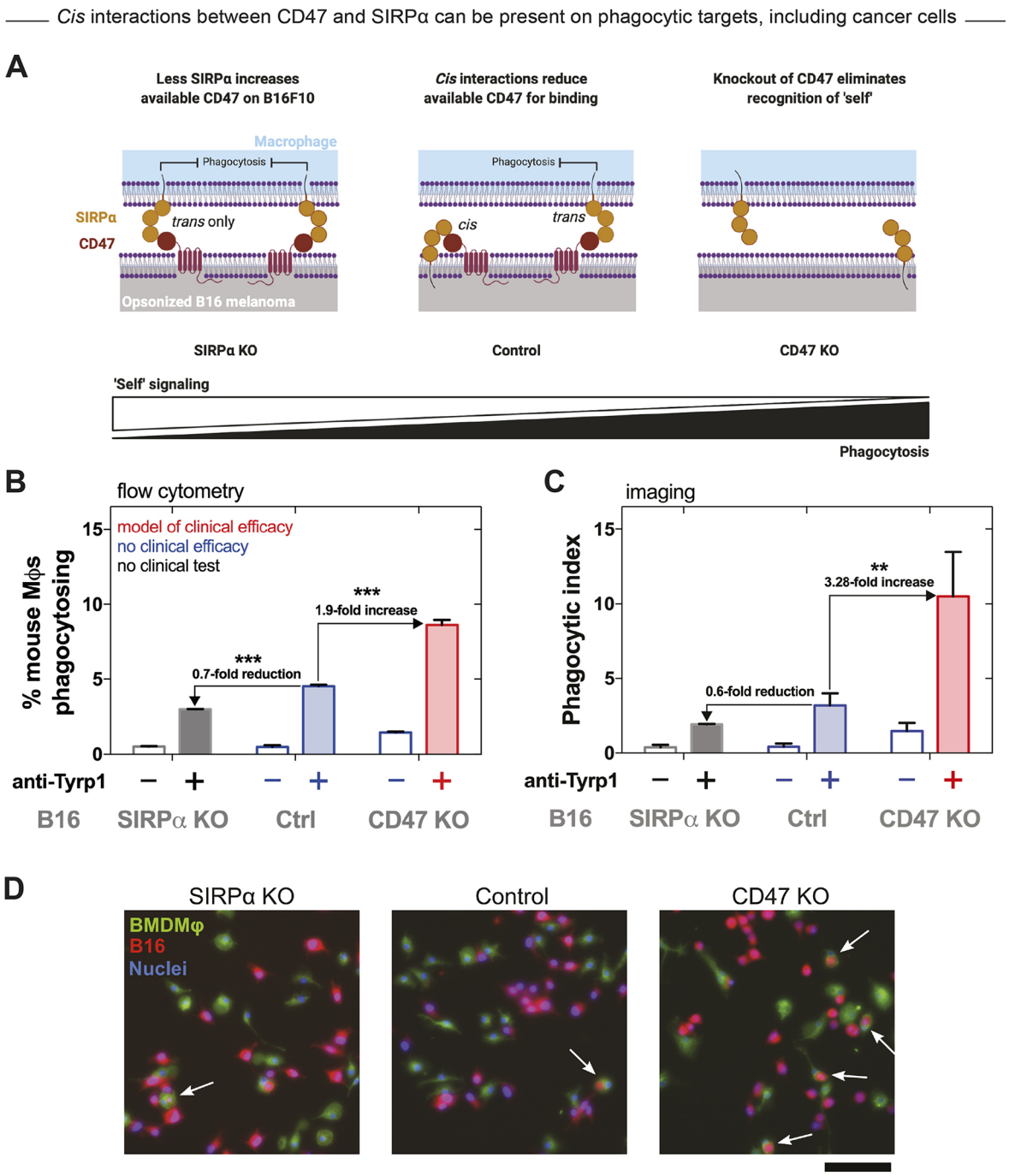

Fig. 3. Knockout of either CD47 or SIRPα on mouse B16 melanoma cells affect CD47 availability to signal 'self' to primary mouse macrophages. (A) A diagram of the hypothesis. Knockout of SIRPα on antibody-opsonized B16 shifts CD47 interactions from *cis* to *trans* interactions, inhibiting phagocytosis of the tumor cell. Knockout of CD47 abolishes 'self' signaling and increases phagocytosis. (B) Primary mouse bone marrow-derived macrophages (BMDMϕs) phagocytose mouse B16 melanoma cells opsonized with anti-Tyrp1 antibody after knockout of indicated protein. Results are mean±s.d. (n=3). ***P<0.001 (one-way ANOVA and post-hoc Bonferroni test). (C) Fluorescence microscopy determinations of the phagocytic index, defined as the percentage of BMDMϕs that are actively engulfing cells multiplied by the number of target cells engulfed per engulfing BMDMϕ. (D) Representative images of BMDMϕs engulfing opsonized B16 melanoma cells. Arrows denote phagocytic events. Scale bar: 100 µm.

SIRPα on cancer cells modulates their engulfment

Numerous cell types express both CD47 and SIRPα, including human A549 lung cancer cells (Fig. 1B) and mouse B16 melanoma cells (Figs S1B and S4A). We hypothesized that with such cells *cis* CD47–SIRPα interactions regulate their phagocytosis by modulating *trans* presentation of 'self' (Fig. 3A), as is relevant to cancer therapy (Fig. 1A). B16 cells were studied to generalize species effects and because they are widely used in preclinical immunotherapy, including CD47–SIRPα blockade (Ingram et al., 2017; Chowdhury et al., 2019; Mandal et al., 2019).

CRISPR/Cas9-mediated knockout (KO) of CD47 or SIRPα was performed in B16 cells, alongside a line with a non-targeting guide RNA for control, and all B16 cells were equally opsonized with anti-Tyrp1 (Figs S1B and S4A) before being added to mouse bone-

marrow derived macrophages (BMDMϕs). Flow cytometry and imaging both show that engulfment of SIRPα-KO cells was reduced by 30–40% relative to control B16s, compared to the 2–3-fold increase for CD47-KO cells (Fig. 3B–D; Fig. S4B); also 1–2 cells were again engulfed per BMDMϕ (Fig. 3C,D). These results support the general hypothesis that CD47–SIRPα *cis* interactions modulate *trans* interactions.

Co-display of CD47–GFP and SIRPα suppresses binding of soluble SIRPα

Heterologous display of human CD47–GFP on Chinese hamster ovary (CHO) cells varies broadly, but the variation includes physiological levels of CD47 (Subramanian et al., 2007). Co-expression (or not) of human SIRPα (unlabeled but expressed similarly) with CD47–GFP, allowed us to assess *trans* binding of anti-CD47 or soluble SIRPα. Co-expressing cells show a ∼90% reduction of the red fluorescence from anti-CD47 binding compared to cells expressing CD47–GFP alone (Fig. 4A,B). Such a reduction is consistent with *cis-trans* competition. For red-fluorescent soluble SIRPα, co-expressing cells showed almost no *trans*-SIRPα binding relative to cells expressing CD47–GFP alone (Fig. 4B). The larger effect on *trans*-SIRPα binding relative to anti-CD47 is consistent with weaker association of SIRPα with CD47.

Simulated SIRPα can bend and bind CD47 in *cis*

Among its three Ig domains, the N-terminal domain of SIRPα binds the single Ig domain of CD47 in a crystallizable interaction (Hatherley et al., 2008). The Ig domains of SIRPα move as near-rigid bodies linked by hinges in computations of normal mode motions (Fig. 4C). Insertion of SIRPα with its transmembrane domain into a simulated lipid bilayer while in crystallographic association with CD47 in the same membrane (Fig. 4D) provides a molecularly detailed view of SIRPα bending over and binding to CD47 in *cis*. Bending energy could destabilize binding energy, and a first step toward determining this might be to relate SIRPα-docking probabilities for CD47-derived 'self' peptides to measured binding affinities (Rodriguez et al., 2013).

Conclusion

Safety of CD47 blockade is a concern across multiple clinical trials, with loss of various blood cells (RBCs, platelets, etc.; see Andrechak et al., 2019). Clearance by macrophages has been claimed to result from opsonizing signals on aged cells (Advani et al., 2018), such as opsonizing IgG (against oxidation-generated epitopes) or membrane rigidity (Sosale et al., 2015). Paradoxically, fresh hRBCs are minimally eaten by macrophages and are not engulfed more when treated with anti-CD47 (Fig. 1C,D). This paradox is resolved by disruption of the inhibitory CD47–SIRPα *cis* interaction on the macrophage. Engulfment clearly increases, even though blocking CD47 on only the macrophage should release SIRPα molecules to conceivably interact in *trans* and increase inhibition. More study is clearly needed, but this is the first study to illustrate the importance of CD47 on the macrophage, with clear implications for clinical blockade of CD47.

The presence of *cis* interacting CD47–SIRPα is surmised from our four experimental approaches, including anti-CD47 on human-derived THP-1 macrophages (Fig. 1C,D; Fig. S2). These approaches are shRNA-mediated knockdown of CD47 on THP-1 macrophages (Fig. 2; Fig. S3), phagocytosis by primary mouse macrophages of mouse melanoma B16 cells with SIRPα or CD47 deleted (Fig. 3; Fig. S4), and heterologous co-display of SIRPα and CD47 (Fig. 4A,B). Simulations further indicate a *cis* interaction is physically reasonable. The potency of the phospho-signaling of SIRPα in *cis* versus that seen in *trans* remains unclear, but phospho-signaling in *trans* saturates with increased CD47 on a target (Tsai and Discher, 2008), which differs from the linearity seen upon knockdown (Fig. 2B) and perhaps reflects a limit to SIRPα accumulation at the phagocytic synapse.

The efficacy of anti-CD47 in human cancer trials depends on macrophage activation, such as with tumor-opsonizing antibodies (Fig. 1Ai) (Advani et al., 2018; Andrechak et al., 2019). Expression of anti-CD47 from bacteria within a mouse tumor might activate macrophages via bacterial pathways (Chowdhury et al., 2019), but the same anti-CD47 is also likely to disrupt CD47–SIRPα *cis* interactions on tumor-associated macrophages and thereby drive hyper-phagocytosis. SIRPα blockade should lead to similarly high activation and hyper-phagocytosis, which is interesting to consider in light of anti-tumor efficacy with systemically injected anti-SIRPα blocked macrophages (Alvey et al., 2017).

MATERIALS AND METHODS

Chemicals

Dulbecco's phosphate-buffered saline (DPBS) without Ca^{2+} or Mg^{2+} (Invitrogen, Carlsbad, CA) was supplemented with either 1% bovine serum albumin (BSA) or 1% BSA and 0.05% Tween 20 (Millipore Sigma, Darmstadt, Germany). Tris-buffered saline (TBS) and TBS with 0.5% Tween 20 (TTBS) were used in western blotting. Hoechst 33342 (Invitrogen) was used for DNA stains.

Antibodies

The anti-human CD47 antibody clones B6H12 (catalog no. 556044, BD Biosciences, San Jose, CA), 2D3 (catalog no. 14-0478-82, Thermo Fisher Scientific, Waltham, MA), and 6H9 (a gift from Marilyn Telen at Duke University, Durham, NC) were used for detection of human CD47 on macrophages or CHO cells expressing full-length human CD47. Quantification of CD47 and SIRPα was performed using B6H12–FITC (catalog no. 556045, BD Biosciences, San Jose, CA) and anti-SIRPα clone SE7C2 (catalog no. sc-23863, Santa Cruz Biotechnology, Dallas, TX), respectively. Human SIRPαex [produced as a secreted and purified SIRPα1-GST as per Subramanian et al. (2007), see below] was used for experiments comparing binding affinities between species. The following antibodies were used as IgG opsonin in our phagocytosis assays: polyclonal rabbit anti-human RBC (referred to as anti-hRBC in the text) (catalog no. 109-4139, Rockland Immunochemicals), polyclonal rabbit anti-sheep RBC (catalog no. 113-4139, Rockland Immunochemicals, Limerick, PA) to target sheep red blood cells (anti-shRBC), rabbit anti-streptavidin (catalog no. S6390-1ML, Sigma-Aldrich), and rabbit anti-streptavidin conjugated to FITC (catalog no. 200-402-0955, Rockland Immunochemicals) to target streptavidin coated polystyrene beads (catalog no. SVP-50-5, Spherotech, Lake Forest, IL). Anti-Cas9 (7A9-3A3 clone) antibody (catalog no. ab191468, Abcam, Cambridge, MA) was used to detect Cas9 expression in transduced cell lines in western blot analysis. Secondary antibodies used for detecting opsonin levels and uningested beads included goat anti-rabbit FITC or goat anti-rabbit F(ab′)2 R-PE (Millipore Sigma). Secondary antibodies used for detecting SIRPαex binding included anti-GST Alexa Fluor 488 (Invitrogen). Secondaries antibodies used for confirming complete RBC engulfment included donkey anti-rabbit Alexa Fluor 647 (Invitrogen). Cytokine granulocyte colony stimulating factor (G-CSF) was purchased from R&D Systems (Minneapolis, MN).

Cell cultures and THP-1 differentiation

COS-1, CHO-K1, A549, THP-1 and B16F10 cells (American Type Culture Collection, Manassas, VA) were maintained in culture with DMEM, MEMα, F-12, RPMI 1640 and RPMI 1640 (Invitrogen), respectively. All cell culture media, unless otherwise specified, was supplemented with 10% (v/v) fetal bovine serum (FBS; F2442, Sigma), 100 U/ml penicillin and 100 µg/ml streptomycin (Gibco, Gaithersburg, MD). Human mesenchymal stem cells (MSCs; Osiris Therapeutics, Columbia, MD) were maintained in

Journal of Cell Science (2020) 133, jcs237800. doi:10.1242/jcs.237800

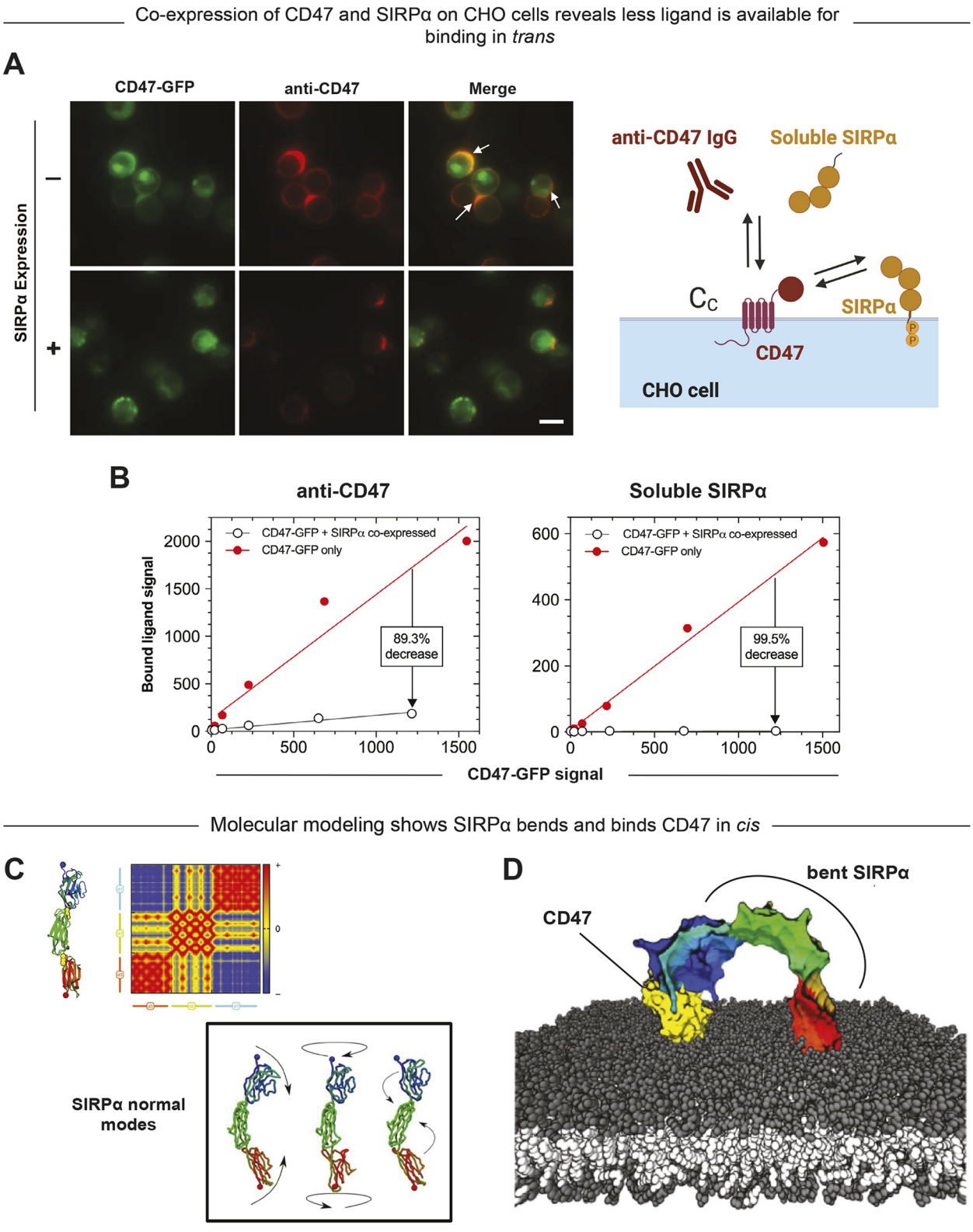

Fig. 4. In heterologous display, CD47–SIRPα *trans* interactions are out-competed by *cis*, and molecular modeling shows SIRPα bends and binds CD47 in *cis*. (A) Images, CHO cells expressing human CD47–GFP were labeled with anti-CD47 as detected with Alexa Fluor 647 secondary antibody. Cells co-displaying full-length human SIRPα suppress anti-CD47 binding. Scale bar: 10 µm. Diagram, anti-CD47 and soluble SIRPα bind membrane-associated CD47 in *trans* while competing with membrane SIRPα. (B) Quantification of anti-CD47 binding to CD47–GFP, and soluble SIRPα (labeled with red fluorophore) binding to CD47–GFP. Flow cytometry shows CD47–GFP levels vary between cells, and bound ligand signal increases proportionately. Co-displayed SIRPα reduces ligand binding in *trans* by >90%, consistent with *cis-trans* competition. Data points were generated by averaging 10,000 events from flow cytometry. (C) Top, the extracellular region of SIRPα in ribbon representation with hinge regions as yellow Cα carbons from Arg-114 to Lys-116, and Arg-220 to Phe-222. The covariance matrix of all Cα carbons is based on the first ten normal modes in a Gaussian network model; bottom, snapshots show the first three modes, highlighting rigid body domains bending and rotating around hinges. (D) Coarse-grained atomistic computation of lipid bilayer with SIRPα binding in *cis* to CD47 (PDB: 2JJS).

low-glucose DMEM, supplemented with 20% (v/v) FBS with the previously mentioned penicillin-streptomycin concentrations. All cell lines were regularly tested for mycoplasma contamination. Cells were detached using 0.05% trypsin and 0.5 mM EDTA (Invitrogen) for passaging. Human blood was obtained from finger pricks of healthy donors. Blood from other species was obtained from Covance (Princeton, NJ) and washed three times in 0.4% BSA. Human hematopoietic stem cells (HSCs) were obtained from fresh purified bone marrow (BM)-derived human $CD34^+$ cells from Lonza (Basel, Switzerland). All HSC experiments were performed in hematopoietic stem cell expansion medium (StemLine-II; Millipore Sigma) and supplemented with 1× antibiotics and G-CSF (100 ng/ml) for 7 days for cultured cells. Peripheral blood monocytes from human donors were obtained through the Human Immunology Core (University of Pennsylvania, Philadelphia, PA).

Differentiation of THP-1 cells followed a protocol based on several recent publications that all refer to the differentiated cells as THP-1 macrophages (Genin et al., 2015; Starr et al., 2018; Sedlyarov et al., 2018). Differentiation was achieved in 100 ng/ml phorbol myristate acetate (PMA) (Millipore Sigma) for 2–3 days, which leads to these cells switching from growth in suspension (as monocytic cells) to attaching to tissue-culture plastic. Gene expression data shown in Fig. S1B confirms that PMA-differentiated THP-1 macrophages and primary macrophages have similar expression profiles for key macrophage markers, while differing greatly from two epithelial cell types.

Expression of human CD47–GFP and SIRPα

Human CD47 (hCD47; isoform 2) was PCR amplified, digested with XhoI and BamHI (New England Biolabs, Ipswich, MA) and ligated to a similarly digested vector pEGFP-N3 (Takara Bio USA, Inc., Mountain View, CA). CHO cells were plated at 1×10^5 cells/cm^2 at 1 day prior to transfection. On the day of transfection, medium was replaced with 2 ml Opti-MEM I (Invitrogen) per 25 cm^2 surface area and 10–15 µl Lipofectamine 2000 and 5 µg plasmid DNA were diluted in 0.25 ml Opti-MEM I separately and, 5 min later, mixed and incubated for a minimum of 20 min at 25°C. Lipid–DNA complexes in a total volume of 0.5 ml Opti-MEM I were added to the flasks and incubated for 4–6 h. The flasks were then replenished with fresh growth medium. Transfected cells were harvested using DPBS supplemented with 2 mM EDTA (Invitrogen) at 1–2 days post transfection for analysis. Full-length human SIRPα was expressed in CHO cells in a similar manner to human CD47–GFP.

Soluble human SIRPα production

COS-1 cells were transfected with pcDNA3-based vector encoding a human SIRPα extracellular domain fused to GST using Lipofectamine 2000 (Invitrogen). Secreted SIRPα1–GST (referred as hSIRPαex) was affinity-purified using glutathione–Sepharose 4B (Amersham Biosciences, Little Chalfont, UK) and dialyzed against DPBS (Invitrogen). The protein was stored at −20°C with or without addition of 10% (v/v) glycerol (Thermo Fisher Scientific).

Production of recombinant human CD47

Plasmid encoding the extracellular domain of human CD47 or mouse CD47 were PCR amplified, digested with XbaI and SalI (New England Biolabs) and ligated to a similarly digested vector, pEF-BOS-XB, which results in an in-frame fusion of CD4d3+4-biotin at the C-terminus of the extracellular domain of CD47. The above vector containing the extracellular domain of CD47 was transfected into CHO-K1 cells using Lipofectamine 2000 (Invitrogen). Secreted CD47-CD4d3+4 was concentrated using a 10 kDa molecular mass cut-off (MWCO) Amicon filter (Millipore Sigma) and biotinylated at the C-terminus using a biotin-protein ligase (Avidity, LLC) and dialyzed against DPBS (Invitrogen). The protein was affinity-purified using a monomeric Avidin (Promega) and dialyzed against DPBS (Invitrogen).

Measurement of human SIRPα and CD47 on cells

Human RBCs, THP-1 cells, A549 cells, peripheral blood monocytes and human MSCs were labeled with 15 µl of B6H12-FITC at saturating levels (BD Biosciences) against human CD47 for 30 min at room temperature. Cells were washed and resuspended in DPBS supplemented with 5% FBS for flow cytometry analysis. For measurement of human SIRPα expression on CHO-K1 cells anti-SIRPα (clone P3C4) (catalog no. LS-C179629, MBL International, Woburn, MA) was used. Anti-human CD47 measurements and detections were performed using different antibodies above recognizing different epitopes of CD47. Saturating concentration of anti-SIRPα or anti-human CD47 antibodies were used as similarly described for the above cells.

Lentiviral knockdown of CD47 in THP-1 cells

shRNA lentiviral supernatants to CD47 were purchased from Millipore Sigma (TRC#: TRCN0000007836, TRCN0000007837) to target CD47 and resulted in 52 and 87% knockdown, respectively. Further details of these clones are available from the Millipore Sigma website. Target THP-1 cells were infected with lentiviral supernatants at a multiplicity of infection (MOI) of 10 in the presence of 80 µg/ml polybrene (hexadimethrine bromide) (Millipore Sigma) and remained in culture for 24 h at 37°C and replaced with fresh RPMI 1640 supplemented with 10% FBS. Cells with integrated viral sequence were selected using puromycin (Millipore Sigma) at 2 µg/ml and then passaged with continuous puromycin selection. The degree of CD47 silencing was regularly monitored by flow cytometry and western blotting with 1:200 anti-SIRPα (clone SE7C2, Santa Cruz Biotechnology). Control cell cultures were generated with control lentivirus in parallel.

CRISPR/Cas9-mediated knockout of CD47 and SIRPα in B16F10 cells

LentiV-cas9_puro and Lenti_sgRNA_EFS_GFP plasmids (Addgene #108100 and 65656, respectively) were gifts from Christopher Vakoc. The single guide RNA (sgRNA) oligonucleotides (CD47, 5′-TCCCCGTAGA-GATTACAATG-3′; SIRPα, 5′-TAATTCTAAGGTCATCTGCG-3′) were designed using the Broad CRISPR algorithm. sgRNAs were cloned into the sgRNA vector using a BsmBI restriction digest.

HEK293T cells were used for lentiviral delivery of Cas9 and sgRNA and cultured in high-glucose DMEM supplemented with 10% (v/v) FBS (F2442, Sigma), 100 U/ml penicillin and 100 µg/ml streptomycin (Gibco). To generate lentivirus, transfer plasmid, pVSVg and psPAX2 were co-transfected into HEK293T cells at a 2:2:1 ratio using Mirus TransIT (MIR6603) transfection reagent (Mirus, Madison, WI) following the manufacturer's protocol. Viral supernatants were collected 48 h after transfection and added to target cells at a 1:1 ratio of culture medium to viral supernatural. Successfully transduced cells were selected using puromycin at 2 µg/ml. Cas9 expression was confirmed using western blot analysis. Clonal knockout cells lines were developed and confirmed using both flow cytometry and western blot analysis using the previously described antibodies.

Binding isotherm for soluble CD47 for wild-type and knockdown THP-1 cells

The binding isotherm of soluble human CD47 was performed for THP-1 wild-type and CD47 knockdowns, as noted, over a range of concentration using flow cytometry. Forward scatter, side scatter and fluorescence (FL1, FL2, FL3, FL4 channels in logarithmic mode) were acquired for at least 10^4 events using a FACScan, FACSCalibur or LSR II (BD Biosciences, San Jose, CA). Data points from flow cytometry were plotted and analyzed using a hyperbolic fit of the form $y=A\,x/(K+x)$ to obtain the K_d values shown.

Kinetics measurements

The rates of association (k_{on}) of SIRPα with soluble CD47 were measured at room temperature. Mixtures of 8, 4 and 2 µM soluble CD47 with 15 µl of B6H12–FITC against human CD47 at saturating levels (BD Biosciences) were pre-equilibrated for 3 h to produce the primary complex. After mixing, aliquots were periodically withdrawn and added to the human THP-1 cells, then washed and diluted in PBS (1:30) to measure the CD47 and SIRPα binding using flow cytometry. Forward scatter, side scatter and fluorescence (FL1, FL2, FL3, FL4 channels in logarithmic mode) were acquired for at least 10^4 events using a FACScan, FACSCalibur or LSR II (BD Biosciences). Data points from flow cytometry were plotted and fitted to obtain the k_{on} values shown.

Phagocytosis assay of human RBCs by PMA-differentiated THP-1 macrophages

For the phagocytosis assays, macrophages were plated in 4 cm^2 Lab-Tek II Chambered Coverglass (Nalge Nunc International, Rochester, NY) or 12-well tissue culture plates (Corning, Corning, NY) at 1×10^5 cells per 4 cm^2. Streptavidin polystyrene beads or RBCs were added to macrophages at a ratio of 20:1 and allowed to incubate at 37°C for 60 min. Non-phagocytosed beads or RBCs were washed with DPBS. For assays using RBCs as targets, lysis of non-ingested RBCs was performed by adding deionized H_2O for 30 s, followed by immediate replacement with 0.4% BSA and fixing with 5% formaldehyde for 5 min.

For stimulated phagocytosis assays, beads (with or without CD47) were incubated with rabbit anti-streptavidin serum, sheep RBCs with rabbit anti-sheep RBC antibody, and human RBCs with rabbit anti-human RBC antibody, respectively, as the opsonin. Beads or RBCs were opsonized at their respectively titrated concentrations for 45 min at room temperature. Opsonized beads and RBCs were washed twice and resuspended in 50 µl of PBS containing 0.4% BSA. If the opsonized target required an additional CD47 block, they were treated with anti-CD47 (B6H12 clone) diluted in DPBS to a final concentration of 0.5 µg/ml for 45 min at room temperature. For phagocytosis assays in which the interactions in *cis* on THP-1 cells was disrupted, we also added 1.5 µM anti-CD47 clone B6H12 antibody to the THP-1 cells prior to the addition of RBCs. The antibody was allowed to bind for 1 h prior to the assay and then washed out with DPBS. Finally, if RBCs were used, they were stained with PKH26 membrane dye (Sigma-Aldrich) for 45 min at room temperature prior to their addition to THP-1 cultures.

To identify non-internalized beads, beads were labeled with a primary antibody, rabbit anti-streptavidin (catalog no. S6390-1ML, Millipore Sigma) at 1:1000 in DPBS for 20 min at 25°C. A second antibody, anti-rabbit IgG conjugated to R-phycoerythrin (R-PE) (catalog no. 52412-1MG-F, Millipore Sigma), was added at 1:1000 in PBS to the cells and incubated for an additional 20 min at 25°C. Cells were then washed with 0.4% BSA and then quantified by light and fluorescence microscopy. For differentiation of non-internalized RBCs, fixed THP-1 cells were blocked with 5% BSA for 30 min followed by addition of donkey anti-rabbit IgG (to target rabbit anti-human RBC) conjugated to Alexa Fluor 647 at 1:500 dilution in DPBS for 45 min at 25°C. Secondary antibody would not be able to bind to completely engulfed RBCs but would stain RBCs that simply adhered to the THP-1 surface. For quantification purposes, we define true phagocytic events as those in which RBCs are completely internalized and do not stain for secondary antibody. At least 200 macrophages were scored per well and experiments were repeated at least three times.

Primary mouse BMDMϕs and phagocytosis of B16 cell lines

Bone marrow cells were isolated from femurs and tibias of healthy male C57BL6/J mice (The Jackson Laboratory 000664) and cultured in 10-cm petri dishes containing Iscove's modified Dulbecco's medium (IMDM, Gibco 12440-053) supplemented with 10% (v/v) FBS, 100 U/ml penicillin, 100 µg/ml streptomycin (Gibco), and 20 ng/ml M-CSF (Biolegend 576404) for 7 days at 37°C, 5% CO_2. All animal experiments were performed according to protocols approved by the University of Pennsylvania's IACUC (protocol #805977 and #804455). The resulting BMDMϕs were detached with 0.05% trypsin-EDTA (TRED, Gibco) and re-plated in 6- or 24-well tissue culture plates at a density of 2.1×10^4 cells/cm^2.

The following day, macrophages were stained with 0.5 µM CellTracker Deep Red (C34565, Thermo Fisher Scientific) for 10 min at 37°C. The labeled BMDMϕs were washed twice with serum-free IMDM. B16 cell lines were labeled with 1 µM CFDA-SE (V12883, Thermo Fisher Scientific) and detached with 0.05% TRED, counted and resuspended at 2×10^5 per ml in serum-free IMDM. Labeled B16 cells were opsonized in suspension with 5 µg/ml anti-Tyrp1 (clone TA99, Bio X Cell BE0151, Lot #715419A1) or mIgG2a isotype control (clone C1.18.4, Bio X Cell BE0085, Lot#692418S1) for 30 min on ice.

For analysis of phagocytosis by flow cytometry, 2 ml ($\sim4\times10^5$) of the CFDA-labeled, opsonized B16 suspension was added to each well of a six-well plate containing Deep Red-labeled BMDMϕs and incubated at 37°C, 5% CO_2 for 2 h. All cells were detached with 0.25% TRED and resuspended in FACS buffer [PBS plus 1% (w/v) BSA and 0.1% sodium azide] and analyzed on an LSRII flow cytometer (BD Biosciences). For analysis of phagocytosis by fluorescence microscopy, 0.5 ml containing opsonized B16 cells was added to each well of a 24-well plate containing Deep Red-labeled BMDMφs and incubated at 37°C, 5% CO_2 for 2 h. For the final 15 min of the incubation period, cells were stained with 1 µg/ml Hoechst 33342 (Thermo Fisher Scientific) before fixation with 4% formaldehyde. Epifluorescence images were acquired on an EVOS FL auto imaging system with either a 20× objective or on an Olympus IX inverted microscope with a 40× objective. For imaging, we quantified the phagocytic index, which is defined as the product of the percentage of the total BMDMϕs population phagocytosing and the number of target cells engulfed per BMDMϕ.

Immunoprecipitation and western blotting

Wild-type THP-1 phagocytes and CD47 knockdowns (2×10^6) were cultured and differentiated in six-well plates for 48 h after PMA differentiation. Human CD47 was attached to 2.1 µm diameter beads at specific densities as described above and added at a bead-to-cell ratio of 20:1 for 10 min. Following the incubation time, the cells were washed with ice-cold PBS and then lysed on ice in 300 µl of lysis buffer [50 mM Tris-HCl (pH 7.4), 150 mM NaCl, 1 mM EDTA, 1% NP-40, 1% protease inhibitor cocktail (Millipore Sigma) and 2 mM activated sodium orthovanadate]. For immunoprecipitation, whole-cell lysate was mixed with 1:200 anti-SIRPα (SE7C2 clone) antibody (Santa Cruz Biotechnology, Inc.) with Pierce Protein G agarose (Thermo Fisher Scientific) at 4°C overnight. Precipitated protein was placed in 4–12% SDS-PAGE gels in MOPS buffer (Invitrogen), transferred onto polyvinylidene difluoride (PVDF) membrane, blocked and labeled via the anti-phospho-tyrosine IgG conjugated to horseradish peroxidase (HRP)- (1:1000, catalog no. ab16389, Abcam) and anti-SIRPα (C-20 clone) (1:500, catalog no. sc-6922, Santa Cruz Biotechnology) primary antibodies and anti-goat-HRP (Amersham Biosciences). All western blots were run in duplicate, along with an additional blot for actin to ensure constant protein load among samples.

Fluorescent labeling of transfected CHO with soluble SIRPα and CD47 antibodies

A mix of 5 µl of soluble SIRPα (final concentration ∼1 µM), 5 µl of 2 mg/ml Alexa Fluor 647-conjugated rabbit anti-GST, 40 µl DPBS, 1% BSA and 2.5×10^6 CHO cells was prepared, and incubated at room temperature for at least 30 min. Cells were pelleted (500 ***g*** for 5 min) and resuspended in 1 ml cold DPBS and analyzed immediately. For antibody labeling, saturating levels of anti-CD47 antibody in 50 µl of DPBS, 1% BSA and 2.5×10^6 CHO cells were mixed together and incubated as above. Cells were washed in 0.5 ml DPBS with 1% BSA and then resuspended in 50 µl of DPBS with 1% BSA containing 5 µl of secondary antibody (2 mg/ml). After incubation for 30 min at room temperature, cells were washed once in 0.5 ml DPBS and resuspended in 1 ml of DPBS with 1% BSA and imaged immediately.

Quantification of fluorescent intensity

Images were acquired with an inverted microscope (Olympus; IX71) with a 60× (oil, 1.4 NA) objective using a Cascade CCD camera (Photometrics, Tuscon, AZ). Image acquisition was performed with Image-Pro Plus software (Media Cybernetics, Silver Spring, MD). All subsequent image analysis was done using ImageJ.

GEO microarray data analysis

Data from the GEO database was used to obtain gene expression data for key genes associated with macrophage identity (Fig. S1B). The cell types included in this analysis were human HEK 293T (GEO accession GSE28715), human PMA-differentiated THP-1 macrophages (GEO accession GDS4258), primary mouse macrophages (GEO accession GDS2454) and mouse B16F10 melanoma (GEO accession GSE33607).

Molecular modeling

To gain insight about the degree of flexibility and mobility of SIRPα, we used the Normal Mode Analysis technique. For this purpose, we used the α-carbon backbone of the published crystal structure for SIRP-α1 as model (PDB: 2WNG). Our first goal was to detect the presence of hinges. This problem is challenging when only one structure is known, and several algorithms and techniques have been developed to tackle such a problem

(Thorpe et al., 2001; Wells et al., 2005; Flores et al., 2006, 2008). Our approximation used the Gaussian Network Model, which assumes that all the residue fluctuations around their equilibrium coordinates are Gaussian (Bahar et al., 1997; Haliloglu et al., 1997). This method has been tested to be suitable to determine structural displacements and consequently backbone motional correlations. By virtue of these correlations, the different domains in the protein are determined as well as the location of the hinges (Kundu et al., 2004). The normal modes were obtained using a rcutoff=15Å. The correlations between them were computed using the following expression:

$$C_{ij} = \frac{\langle \Delta r_i \cdot \Delta r_j \rangle}{\sqrt{\langle \Delta r_i^2 \rangle \langle \Delta r_j^2 \rangle}}$$

where Δr_i is the total displacement of the α-carbon of the *i*-th residue from its equilibrium position due to the first n normal modes, and

$$\langle \Delta r_i \cdot \Delta r_j \rangle = \sum_{k=1}^{n} \frac{\kappa_B T}{\omega_\kappa^2} \frac{L_{ik} L_{jk}}{\sqrt{m_i m_j}}$$

where ω_κ^2 is the frequency of the *k*-th normal mode and L_{ik} is the displacement of the α-carbon of residue *i* due to normal mode *k*.

The cylindrical shape of the protein in the crystal structure yields normal modes that are very close in energy, but three different regions emerge in the normal mode analysis matrix and unsurprisingly correspond to the three Ig domains in the crystal structure. The regions along the diagonal of the matrix with values close to zero (i.e. regions with reduced mobilities) are expected to behave as hinges (Flores et al., 2008). In this way, we can determine that the regions delimited by residues 113–117 and 220–222 act as hinges. Since we were also interested in having a spatial description of the normal modes, we needed to make use of the Anisotropic Network Model (ANM) (Hinsen et al., 1999). Despite being less realistic than GNM, we used ANM since it is better suited for assessing the directions of motions (Cui and Bahar, 2007).

Quantitation and statistical analysis

All statistical analyses were performed using GraphPad Prism 7. Unless otherwise noted, all statistical comparisons were made by unpaired two-tailed Student's *t*-test and were considered significant if $P<0.05$. Unless otherwise stated, all plots show mean±s.e.m. or mean±s.d. Figure legends specify the exact meaning of '*n*' for each figure.

Acknowledgements

We thank Jason Andrechak (Penn) for helpful discussions in manuscript preparation. We thank the University of Pennsylvania Flow Cytometry & Cell Sorting Facility and Cell & Developmental Microscopy Core for providing instrumentation and technical assistance in the experiments performed in this study. Any opinions, findings, and conclusions or recommendations expressed in this material are those of the author(s) and do not necessarily reflect the views of the National Institutes of Health, National Science Foundation, and other funding agencies.

Competing interests

The authors declare no competing or financial interests.

Author contributions

Conceptualization: D.E.D., B.H.H., R.K.T., L.J.D., D.P.; Methodology: D.E.D., B.H.H., R.K.T., L.J.D., S.K., J.Y.L., D.P., P.L.R., S.S., J.-W.S.; Software: D.P.; Validation: D.E.D., B.H.H., R.K.T., L.J.D., S.K., J.Y.L., D.P.; Formal analysis: D.E.D., B.H.H., R.K.T., L.J.D., S.K., J.Y.L., D.P., S.S., J.-W.S.; Investigation: B.H.H., R.K.T., L.J.D., D.P., P.L.R., S.S., J.-W.S.; Resources: D.E.D.; Data curation: B.H.H., R.K.T., L.J.D., D.P.; Writing - original draft: D.E.D., B.H.H., R.K.T., D.P.; Writing - review & editing: D.E.D., B.H.H., L.J.D.; Visualization: B.H.H., D.P.; Supervision: D.E.D.; Project administration: D.E.D.; Funding acquisition: D.E.D., B.H.H., L.J.D.

Funding

We gratefully acknowledge support from the National Institutes of Health/National Cancer Institute PSOC Award U54 CA193417, National Heart Lung and Blood Institute Awards R01 HL124106, National Science Foundation Materials Science and Engineering Center grant and CEMB grant to the University of Pennsylvania, the US–Israel Binational Science Foundation, and the Human Frontier Science Program (HFSP) RGP-0024. B.H.H. was supported by the National Science Foundation Graduate Research Fellowship Program under Grant No. DGE-1845298. L.J.D. was supported by a National Institutes of Health/National Cancer Institute NRSA Postdoctoral Fellowship F32 CA228285. Deposited in PMC for release after 12 months.

Supplementary information

Supplementary information available online at http://jcs.biologists.org/lookup/doi/10.1242/jcs.237800.supplemental

Peer review history

The peer review history is available online at https://jcs.biologists.org/lookup/doi/10.1242/jcs.237800.reviewer-comments.pdf

References

Advani, R., Flinn, I., Popplewell, L., Forero, A., Bartlett, N. L., Ghosh, N., Kline, J., Roschewski, M., LaCasce, A., Collins, G. P. et al. (2018). CD47 blockade by Hu5F9-G4 and Rituximab in non-Hodgkin's LYMPHOMA. *N. Engl. J. Med.* **379**, 1711-1721. doi:10.1056/NEJMoa1807315

Alvey, C. M., Spinler, K. R., Irianto, J., Pfeifer, C. R., Hayes, B., Xia, Y., Cho, S., Dingal, P. C. P. D., Hsu, J., Smith, L. et al. (2017). SIRPA-inhibited, marrow-derived macrophages engorge, accumulate, and differentiate in antibody-targeted regression of solid tumors. *Curr. Biol.* **27**, 2065-2077.e6. doi:10.1016/j.cub.2017.06.005

Andrechak, J. C., Dooling, L. J. and Discher, D. E. (2019). The macrophage checkpoint CD47:SIRPα for recognition of 'self' cells: from clinical trials of blocking antibodies to mechanobiological fundamentals. *Philos. Trans. R. Soc. B Biol. Sci.* **374**, 20180217. doi:10.1098/rstb.2018.0217

Bahar, I., Atilgan, A. R. and Erman, B. (1997). Direct evaluation of thermal fluctuations in proteins using a single-parameter harmonic potential. *Fold. Des.* **2**, 173-181. doi:10.1016/S1359-0278(97)00024-2

Bakalar, M. H., Joffe, A. M., Schmid, E. M., Son, S., Podolski, M. and Fletcher, D. A. (2018). Size-dependent segregation controls macrophage phagocytosis of antibody-opsonized targets. *Cell* **174**, 131-142.e13. doi:10.1016/j.cell.2018.05.059

Borghaei, H., Paz-Ares, L., Horn, L., Spigel, D. R., Steins, M., Ready, N. E., Chow, L. Q., Vokes, E. E., Felip, E., Holgado, E. et al. (2015). Nivolumab versus Docetaxel in advanced nonsquamous non–small-cell lung cancer. *N. Engl. J. Med.* **373**, 1627-1639. doi:10.1056/NEJMoa1507643

Chowdhury, S., Castro, S., Coker, C., Hinchliffe, T. E., Arpaia, N. and Danino, T. (2019). Programmable bacteria induce durable tumor regression and systemic antitumor immunity. *Nat. Med.* **25**, 1057-1063. doi:10.1038/s41591-019-0498-z

Cui, Q. and Bahar, I. (2007). Normal mode analysis theoretical and applications to biological and chemical systems. *Brief. Bioinform.* **8**, 378-379. doi:10.1093/bib/bbm010

Doucey, M.-A., Scarpellino, L., Zimmer, J., Guillaume, P., Luescher, I. F., Bron, C. and Held, W. (2004). Cis association of Ly49A with MHC class I restricts natural killer cell inhibition. *Nat. Immunol.* **5**, 328-336. doi:10.1038/ni1043

Flores, S., Echols, N., Milburn, D., Hespenheide, B., Keating, K., Lu, J., Wells, S., Yu, E. Z., Thorpe, M. and Gerstein, M. (2006). The database of macromolecular motions: new features added at the decade mark. *Nucleic Acids Res.* **34**, D296-D301. doi:10.1093/nar/gkj046

Flores, S. C., Keating, K. S., Painter, J., Morcos, F., Nguyen, K., Merritt, E. A., Kuhn, L. A. and Gerstein, M. B. (2008). HingeMaster: normal mode hinge prediction approach and integration of complementary predictors. *Proteins Struct. Funct. Bioinform.* **73**, 299-319. doi:10.1002/prot.22060

Genin, M., Clement, F., Fattaccioli, A., Raes, M. and Michiels, C. (2015). M1 and M2 macrophages derived from THP-1 cells differentially modulate the response of cancer cells to etoposide. *BMC Cancer* **15**, 577. doi:10.1186/s12885-015-1546-9

Haliloglu, T., Bahar, I. and Erman, B. (1997). Gaussian dynamics of folded proteins. *Phys. Rev. Lett.* 79, 3090-3093. doi:10.1103/PhysRevLett.79.3090

Hatherley, D., Graham, S. C., Turner, J., Harlos, K., Stuart, D. I. and Barclay, A. N. (2008). Paired receptor specificity explained by structures of signal regulatory proteins alone and complexed with CD47. *Mol. Cell* **31**, 266-277. doi:10.1016/j.molcel.2008.05.026

Hinsen, K., Thomas, A. and Field, M. J. (1999). Analysis of domain motions in large proteins. *Proteins Struct. Funct. Bioinform.* **4**, 369-382. doi:10.1002/(SICI)1097-0134(19990215)34:3<369::AID-PROT9>3.0.CO;2-F

Ide, K., Wang, H., Tahara, H., Liu, J., Wang, X., Asahara, T., Sykes, M., Yang, Y.-G. and Ohdan, H. (2007). Role for CD47-SIRPalpha signaling in xenograft rejection by macrophages. *Proc. Natl. Acad. Sci. USA* **104**, 5062-5066. doi:10.1073/pnas.0609661104

Ingram, J. R., Blomberg, O. S., Sockolosky, J. T., Ali, L., Schmidt, F. I., Pishesha, N., Espinosa, C., Dougan, S. K., Garcia, K. C., Ploegh, H. L. et al. (2017). Localized CD47 blockade enhances immunotherapy for murine melanoma. *Proc. Natl. Acad. Sci. USA* **114**, 10184-10189. doi:10.1073/pnas.1710776114

Kundu, S., Sorensen, D. C. and Phillips, G. N.Jr. (2004). Automatic domain decomposition of proteins by a Gaussian Network Model. *Proteins Struct. Funct. Bioinform.* 57, 725-733. doi:10.1002/prot.20268

Lopes, F. B., Bálint, Š., Valvo, S., Felce, J. H., Hessel, E. M., Dustin, M. L. and Davis, D. M. (2017). Membrane nanoclusters of FcγRI segregate from inhibitory SIRPα upon activation of human macrophages. *J. Cell Biol.* **216**, 1123. doi:10.1083/jcb.201608094

Mandal, R., Samstein, R. M., Lee, K.-W., Havel, J. J., Wang, H., Krishna, C., Sabio, E. Y., Makarov, V., Kuo, F., Blecua, P. et al. (2019). Genetic diversity of tumors with mismatch repair deficiency influences anti–PD-1 immunotherapy response. *Science* **364**, 485. doi:10.1126/science.aau0447

Montalvao, F., Garcia, Z., Celli, S., Breart, B., Deeguiine, J., Van Rooijen, N. and Bousso, P. (2013). The mechanism of anti-CD20-mediated B cell depletion revealed by intravital imaging. *J. Clin. Invest.* **123**, 5098-5103. doi:10.1172/JCI70972

Oldenborg, P.-A., Zheleznyak, A., Fang, Y.-F., Lagenaur, C. F., Gresham, H. D. and Lindberg, F. P. (2000). Role of CD47 as a Marker of Self on Red Blood Cells. *Science* **288**, 2051. doi:10.1126/science.288.5473.2051

Oldenborg, P.-A., Gresham, H. D., Chen, Y., Izui, S. and Lindberg, F. P. (2002). Lethal autoimmune hemolytic anemia in CD47-deficient nonobese diabetic (NOD) mice. *Blood* **99**, 3500. doi:10.1182/blood.V99.10.3500

Rodriguez, P. L., Harada, T., Christian, D. A., Pantano, D. A., Tsai, R. K. and Discher, D. E. (2013). Minimal "Self" peptides that inhibit phagocytic clearance and enhance delivery of nanoparticles. *Science* **339**, 971-975. doi:10.1126/science.1229568

Sedlyarov, V., Eichner, R., Girardi, E., Essletzbichler, P., Goldmann, U., Nunes-Hasler, P., Srndic, I., Moskovskich, A., Heinz, L. X., Kartnig, F. et al. (2018). The bicarbonate transporter SLC4A7 plays a key role in macrophage phagosome acidification. *Cell Host Microbe* **23**, 766-774.e5. doi:10.1016/j.chom.2018.04.013

Shin, J.-W., Spinler, K. R., Swift, J., Chasis, J. A., Mohandas, N. and Discher, D. E. (2013). Lamins regulate cell trafficking and lineage maturation of adult human hematopoietic cells. *Proc. Natl. Acad. Sci. USA* **110**, 18892-18897. doi:10.1073/pnas.1304996110

Sikic, B. I., Lakhani, N. J., Patnaik, A., Shah, S., Chandana, S. R., Rasco, D. W., Colevas, A. D., O'Rourke, T. J., Papadopoulos, K. P., Fisher, G. A. et al. (2018). A first-in-class, first-in-human phase 1 pharmacokinetic (PK) and pharmacodynamic (PD) study of Hu5F9-G4, an anti-CD47 monoclonal antibody (mAb), in patients with advanced solid tumors. *JCO* **36**, 3002. doi:10.1200/JCO.2018.36.15_suppl.3002

Sosale, N. G., Rouhiparkouhi, T., Bradshaw, A. M., Dimova, R., Lipowsky, R. and Discher, D. E. (2015). Cell rigidity and shape override CD47's "self"-signaling in phagocytosis by hyperactivating myosin-II. *Blood* **125**, 542-552. doi:10.1182/blood-2014-06-585299

Sosale, N. G., Ivanovska, I. I., Tsai, R. K., Swift, J., Hsu, J. W., Alvey, C. M., Zoltick, P. W. and Discher, D. E. (2016). "Marker of Self" CD47 on lentiviral vectors decreases macrophage-mediated clearance and increases delivery to SIRPA-expressing lung carcinoma tumors. *Mol. Ther. Methods Clin. Dev.* **3**, 16080. doi:10.1038/mtm.2016.80

Starr, T., Bauler, T. J., Malik-Kale, P. and Steele-Mortimer, O. (2018). The phorbol 12-myristate-13-acetate differentiation protocol is critical to the interaction of THP-1 macrophages with Salmonella Typhimurium. *PLoS ONE* **13**, e0193601. doi:10.1371/journal.pone.0193601

Subramanian, S., Boder, E. T. and Discher, D. E. (2007). Phylogenetic divergence of CD47 interactions with human signal regulatory protein α reveals locus of species specificity: implications for the binding site. *J. Biol. Chem.* **282**, 1805-1818. doi:10.1074/jbc.M603923200

Thorpe, M. F., Lei, M., Rader, A. J., Jacobs, D. J. and Kuhn, L. A. (2001). Protein flexibility and dynamics using constraint theory. *J. Mol. Graph. Model.* **19**, 60-69. doi:10.1016/S1093-3263(00)00122-4

Tsai, R. K. and Discher, D. E. (2008). Inhibition of "self" engulfment through deactivation of myosin-II at the phagocytic synapse between human cells. *J. Cell Biol.* **180**, 989. doi:10.1083/jcb.200708043

Veillette, A., Thibaudeau, E. and Latour, S. (1998). High expression of inhibitory receptor SHPS-1 and its association with protein-tyrosine phosphatase SHP-1 in macrophages. *J. Biol. Chem.* **273**, 22719-22728. doi:10.1074/jbc.273.35.22719

Vogel, W., Grünebach, F., Messam, C. A., Kanz, L., Brugger, W. and Bühring, H. J. (2003). Heterogeneity among human bone marrow-derived mesenchymal stem cells and neural progenitor cells. *Haematologica* **88**, 126-133.

Weiskopf, K., Ring, A. M., Ho, C. C. M., Volkmer, J.-P., Levin, A. M., Volkmer, A. K., Özkan, E., Fernhoff, N. B., van de Rijn, M., Weissman, I. L. et al. (2013). Engineered SIRPα variants as immunotherapeutic adjuvants to anticancer antibodies. *Science* **341**, 88-91. doi:10.1126/science.1238856

Wells, S., Menor, S., Hespenheide, B. and Thorpe, M. F. (2005). Constrained geometric simulation of diffusive motion in proteins. *Phys. Biol.* **2**, S127-S136. doi:10.1088/1478-3975/2/4/S07